Organic Electronics 13 (2012) 2763–2772

Contents lists available at SciVerse ScienceDirect

Organic Electronics

journal homepage: www.elsevier.com/locate/orgel

Theoretical insights into the charge transport in perylene diimides based n-type organic semiconductors

Lili Lin [a], Hua Geng [b], Zhigang Shuai [c,*], Yi Luo [a,d]

[a] Department of Theoretical Chemistry and Biology, School of Biotechnology, Royal Institute of Technology, S-10691 Stockholm, Sweden
[b] Key Laboratory of Organic Solids, Beijing National Laboratory for Molecular Sciences (BNLMS), Institute of Chemistry, Chinese Academy of Sciences, 100190 Beijing, China
[c] Department of Chemistry, Tsinghua University, 100084 Beijing, China
[d] Hefei National Laboratory for Physical Sciences at the Microscale, University of Science and Technology of China, 230026 Hefei, China

ARTICLE INFO

Article history:
Received 12 June 2012
Received in revised form 1 August 2012
Accepted 1 August 2012
Available online 22 August 2012

Keywords:
n-Type organic semiconductor
Quantum rate equation
Mobility
Substitute groups

ABSTRACT

We employed a tunneling enabled hopping model to investigate the charge transport properties for four n-type organic semiconductors perylene diimides compounds. The molecular parameters are calculated by density functional theory and the transport is modeled by kinetic Monte Carlo simulation. It is found that the substitutions at the bay positions of the perylene core have large influences on the charge transport properties through modifications in molecular conformation, the charge reorganization energy as well as the stacking networks in the crystals. The temperature dependence of the mobility shows typical "band-like", in agreement with the recent experiment, but we ascribe it to be the characteristic of nuclear tunneling effect for a localized charge, not by a delocalized band. The largest charge mobility is calculated to be 16.96 cm^2/V s for the cyano substitution, in good comparison with the experimental value of 6 cm^2/V s.

© 2012 Elsevier B.V. All rights reserved.

1. Introduction

There have been tremendous progresses in design and synthesis of new molecular or polymeric organic semiconductor materials. Many p-type organic materials have been proven to have large charge mobility comparable with, even larger than, the amorphous or polycrystalline silicon [1–5]. It has been noted that efforts should be devoted to n-type organic materials owing to the relatively small mobility and poor air stability. Progresses have been achieved in this direction, for instance, cyclohexyl substituted naphthalene diimides (NDI) has been found to be an n-type semiconductor with high electron mobility (7.5 cm^2/V s) [6]. For the fullerene (C_{60}), the mobility has reached as high as 6.0 cm^2/V s for the device with polymer as dielectric layer [7–9]. Perylene tetracarboxylic diimides (PTCDIs) are also another extensively investigated n-type semiconductor. Many derivatives of the PTCDI have been designed, synthesized and characterized to have good conducting properties [10–19]. Usually, the chemical substitutions on the PTCDI are mainly located either at the end sites or at the core positions. It is commonly thought that the end substitutions can not only improve the solubility but also the air stability, e.g. the long chain alkanes prevent the invasion of H_2O and O_2 to some extent. The core functionalizations are believed to affect the delocalization of electrons and significantly change the stacking configurations in crystals [20].

In this study, we focus on the effect of the core substitution on charge mobility of PTCDI with the same end substitutions (e.g. $CH_2C_3F_7$). For the sake of comparison, four types of compounds with different electron withdrawing substitution groups are investigated (see Fig. 1). With the small changes on the substitution groups at the core, the measured mobility values vary from 0.003 to 6.0 cm^2/V s.

* Corresponding author.
E-mail address: zgshuai@tsinghua.edu.cn (Z. Shuai).

1566-1199/$ - see front matter © 2012 Elsevier B.V. All rights reserved.
http://dx.doi.org/10.1016/j.orgel.2012.08.001

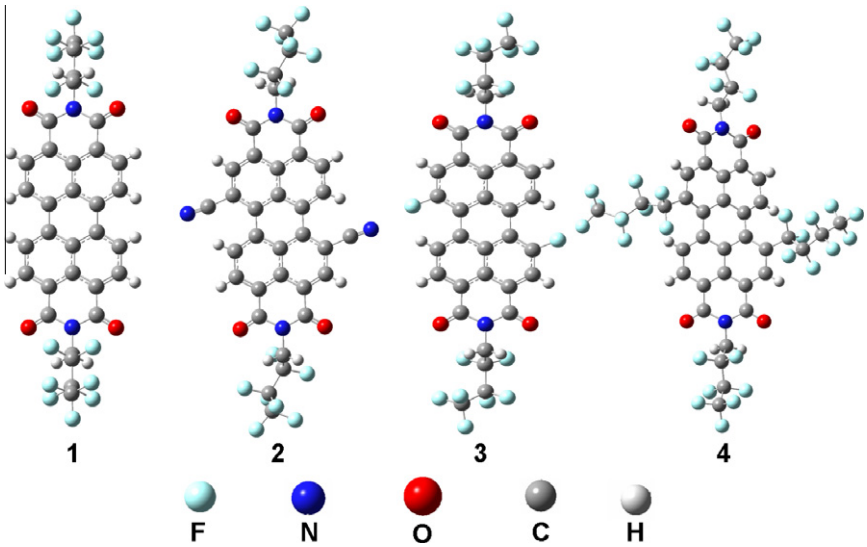

Fig. 1. Molecular structures of four substituted PTCDIs.

Why and how such small modification in substitution in the core of PTCDI can induce such a significant change of charge mobility is still not understood.

In this work, we employ a "tunneling enabled hopping" model [22] coupled with quantum chemistry calculation to study the charge transport in substituted PTCDIs. Under such model, the charge is assumed to be localized on a single molecule, or a small polaron. The hopping from one molecule to another is described by a charge transfer process containing nuclear tunneling effect [22]. The macroscopic transport property is obtained by subsequent dynamic Monte Carlo simulation [23]. All the parameters are obtained by density functional theory, rendering such multiscale approach "first-principles", namely, parameter-free. In this way, the structure–property relationship can be fully explored through computational studies.

2. Methodology

Based on the displaced harmonic oscillator model and the Condon approximation, the quantum charge transfer rate can be deduced from the Fermi Golden Rule [21–23]:

$$k_{fi} = \frac{V_{fi}^2}{\hbar^2}\int_{-\infty}^{+\infty} dt \exp \times \left\{ iE_{fi}t - \sum_j S_j\left[(1+2\bar{n}_j) - e^{i\omega_j t}(1+\bar{n}_j) - e^{-i\omega_j t}\bar{n}_j\right]\right\} \quad (1)$$

where E_{fi} is the potential energy difference between the final state and the initial state and it equals to zero for the self-exchange reaction. Here ω_j is the vibration frequency of the vibration mode j and V_{fi} is the transfer integral. S_j is the Huang–Rhys factor, which can reflect the strength of the electron–phonon coupling, and it is defined as $S_j = \frac{\omega_j \Delta Q_j^2}{2\hbar}$. $\bar{n}_j$ is the averaged phonon occupation number for the j-th normal node $\bar{n}_j = \frac{1}{e^{\frac{\hbar\omega_j}{k_B T}}-1}$.

The electron transfer integral V_{fi}, vibration frequency ω_j and Huang–Rhys factor S_j are important parameters to determine the transfer rate. There are many different approaches to calculate the transfer integral such as the energy splitting method [24–26], the site energy correction method [27–29], the direct coupling method [30–31,22] and so on. Here we adopt the site energy correction method which has been proven to be reliable and easy to be adopted [23,32]. We use the density functional theory (DFT) with the PW91PW91 functional and 6-31G* basis set to describe the electronic structure. The vibration frequencies and the normal coordinates of the neutral and anion states are calculated using the *Gaussian* 09 program [33] with the B3LYP functional and the 6-31G* basis set, then the DUSHIN program [34] is used to calculate the Huang–Rhys factor and reorganization energy for every vibration mode. The total reorganization energy is the sum of the relaxation energy of normal modes:

$$\lambda = \sum_i \lambda_i = \sum_i \frac{1}{2}\omega_i^2 \Delta Q_i^2 = \sum_i \hbar S_i \omega_i \quad (2)$$

Such expression can be termed as normal mode analysis method (NM) [34]. The easiest way to calculate the total reorganization energy is the four-point method based on adiabatic potential energy surface method (AP) [4]. Furthermore, the reorganization energy can also be decomposed onto the internal coordinates to analysis the contributions from different components:

$$\lambda = \sum_i \lambda_i(S_i) = \sum_i \sum_j \frac{1}{2\omega_i}(\alpha_{ij}^2 \Delta S_j^2 + \sum_{m(\neq j)} \alpha_{ij}\alpha_{im}\Delta S_j \Delta S_m) \quad (3)$$

which is deduced according to the relationship:

$$\Delta Q_i = \sum_j \alpha_{ij} \Delta S_j \quad (4)$$

where Q_i is the normal coordinate and S_j is the internal coordinate, for details see the reference of Geng et al. [35].

In our work, the kinetic Monte Carlo simulation approach is adopted to calculate the charge diffusion process based on the microscopic charge transfer rate in organic molecular single-crystals. By repeating the process for thousands of times, we can get thousands of trajectories. The average value of all the trajectories with respect to the time has a linear relationship. The ratio is the diffusion coefficient according to $D = \lim_{t\to\infty} \frac{r^2}{2nt}$, where r and t are the averaged displacement and total time span. n represents the dimension of the charge transport in the crystal. In our calculation, the $10 \times 10 \times 10$ supercell is adopted. The limit time for every track was set as 0.1 ns and 3000 trajectories were chosen to get the average value of the diffusion coefficient D. The charge mobility was finally calculated according to the Einstein equation $\mu = \frac{eD}{K_B T}$.

3. Results and discussion

3.1. Geometric comparison

First, we look at the substitution effects on the molecular structures [14,15,17]. From the single crystal structure, it is seen that the dihedral angles of the skeleton change a lot due to the substitution of electron-drawing groups in the bay positions of the PTCDI molecule (see Fig. 2 and Table 1). For **1**, the planarity is kept with the dihedral angle only about 1.5°. For **2** and **3**, the planarity of the conjugated core has been influenced to some extent due to the substitution at the bay positions with dihedral angles about 5.1° and 3.7°, respectively. The dihedral angle becomes as large as 29.55° in **4**, and its planarity has been totally destroyed owing to the steric encumbrance of the long chain substitution at the bay positions. Besides the planarity differences induced by the substitution at bay positions, the chains connected to the nitrogen atom at the end positions also differ with each other significantly in different systems. For **1**, the four carbon atoms in the chain keep good planarity with the nitrogen atom. Large torsional angles between plane 11-12-13 and plane 12-13-14 have been found in **2** and **4** with the dihedral angles 145.94° and 159.47°. The dihedral angles of plane 12-13-14 and plane 13-14-15 are also as large as 168.93° and 164.32° for **2** and **4**. For **3**, the first dihedral angle (11-12-13-14) is very small with relatively good planarity, while the second dihedral angle (12-13-14-15) is as large as 63.48°. Due to the torsion of the CF_2 group next to the CH_2 group, the angle 11-12-13 increases almost 3.0° in **2** and **4** compared with **1** and **3**. For the same reason, the torsion angle of the CF_2 group which is second closest to the CH_2 group in **3** increases almost 3.0° compared with **1**.

To calculate the reorganization energy, we first optimized the four molecules of neutral and anion states in the gas phase respectively. It is found that, for **1** and **3**, there is no significant change in the gas phase compared with that in crystal phase except the increment of the C–H bond lengths for about 0.1 Å. For **4**, the dihedral angles of 5-1-2-6 and 7-3-4-8 is about 25.47° and 25.33° respectively in the gas phase, which is a little smaller than that in crystal phase (26.53° and 29.55°), that is to say, the core is still non-planar in the gas phase. For **2**, the optimized configuration differs significantly with the structure obtained from the experiment. The core no longer keeps planar in the gas phase with the 5-1-2-6 dihedral angle 16.13°. In addition, the dihedral angles of 11-12-13-14 and 12-13-14-15 in $CH_2C_3F_7$ chains increase to 178.60° and 179.30° respectively. The significant differences of the configurations in the gas phase and the crystal phase indicate that the intermolecular interaction in the crystal is strong enough to change the molecular configurations. The reorganization energy in the crystal can be approximated by that calculated in the gas phase theoretically, significant configuration differences between this two phases may induce drastic errors. Therefore we optimized the molecule (**2**) with the dihedral angles of 5-1-2-6 and 7-3-4-8 all frozen in both the neutral state and the anion state to simulate the crystal structures and to calculate the reorganization energy.

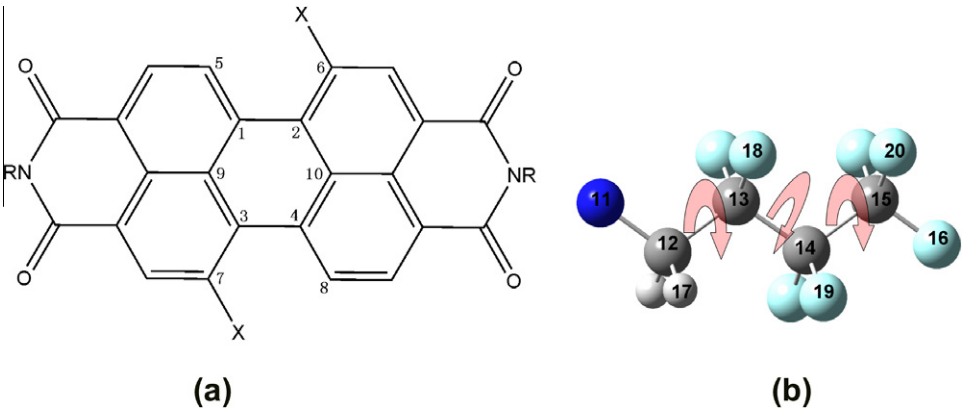

Fig. 2. (a) Structure scheme of systems investigated. $R = CH_2C_3F_7$, X = H (1); X = CN (2); X = F (3); $X = C_4F_9$ (4). (b) Configuration of the R substitution.

Table 1
Conformation differences of four systems in crystal structures (unit: degree).

Internal coordinate	1	2	3	4
5-1-2-6	1.54	5.14	3.74	26.53
7-3-4-8	1.52	5.16	3.74	29.55
9-1-2-10	0.70	2.10	1.87	28.00
9-3-4-10	0.72	2.10	1.87	32.01
11-12-13-14	179.58	145.94	178.51	159.47
12-13-14-15	179.58	168.93	63.48	164.32
11-12-13	109.20	112.63	110.64	112.90
12-13-14	113.55	112.58	115.99	112.69

3.2. Electronic structure

Based on the optimized configurations of the neutral state in the gas phase, the energy levels as well as the electron distribution of the highest occupied molecular orbital (HOMO) and the lowest unoccupied molecular orbital (LUMO) are plotted in Fig. 3. It is straightforward to see that substitutions with electron-withdrawing groups at the bay positions can lower both the energy of the HOMO and the LUMO. The energy levels of the LUMOs of compound **2** and **4** are even lower than −4.0 eV, which means high air stability can be obtained for these two single crystals for n-type doping. The electron distribution of the HOMOs or LUMOs for the four systems is very similar and they are mainly delocalized at the perylene core. For compound **2** and **3**, there is also electron distribution at the substitution groups CN and F. The electron distribution in compound **2** become more delocalized owing to the existence of the π electrons in the CN group. The nonbonding character on the CN group in the compound **2** will induce less bond length adjustment, thus less reorganization energy is expected [36].

The spin density analysis also supports our conclusions. From the spin density distribution of the anions (as illustrated in Fig. 4), we can see that the spin density of molecule **3** and **4** is quite similar to that in molecule **1**. There is little distribution on the core substitutes (F and C_4F_9). The electron on the molecule with the CN group (**2**) has quite significant distribution on the CN group and different signs for the carbon atom and the nitrogen atom in the CN group. That is to say, the electron distribution becomes more delocalized in molecule **2**.

3.3. Molecular charge reorganization energy

The molecular charge reorganization energy strongly depends on the configuration differences between neutral and anion states. Comparison of the configurations between the neutral state and the anion state can reflect the reorganization energy to some extent but not very obviously. Here we perform the calculation of the reorganization energy through the normal mode analysis (NM) to see the contribution of every vibration mode. The contribution to the reorganization energy of all the vibration modes for compound **2** both in the neutral state and the anion state is shown in Fig. 5. The distribution profiles in both the neutral and anion states are similar with one group in the low frequency region (around 500 cm^{-1}) and the other group in the high frequency area (around 1500 cm^{-1}). The contribution from the high frequency area is much larger than that from the low frequency modes. From careful analysis, we found that the vibration modes with the highest contribution to the reorganization energy in both the neutral and anion states mainly come from the C=C in-plane stretching vibration in the core. Similar distribution of the contributions to the reorganization energy of vibration modes can also be seen in other three systems.

The total reorganization energies are shown in Table 2. It shows that compound **2** possesses less reorganization energy than compound **1**, while compound **4** has much larger reorganization energy. The increment of the reorganization in compound **4** is induced by the increase of the degrees of the freedom when the perfluoroalkyl substitutes are introduced. However, the decrease of the reorganization energy in **2** is believed to come from the nonbonding character induced by the CN group [36]. For compound **3**, the total reorganization energy is comparable with that

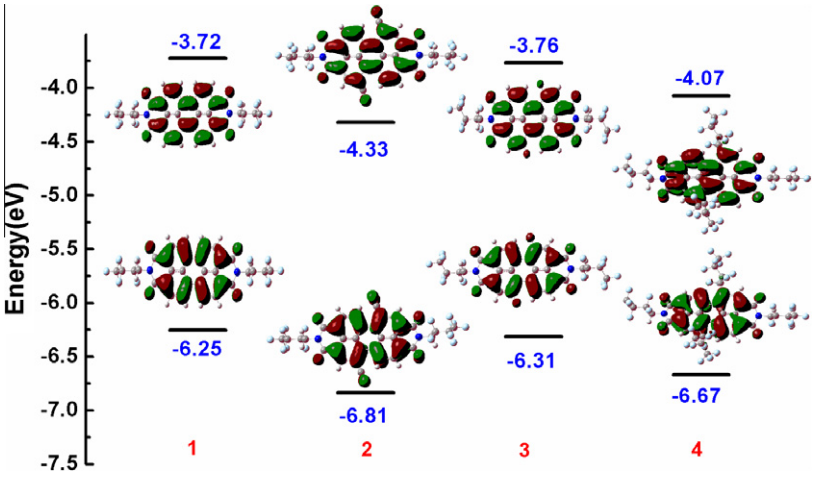

Fig. 3. Energy levels as well as charge density distribution of the HOMOs and LUMOs of compound **1**–**4**.

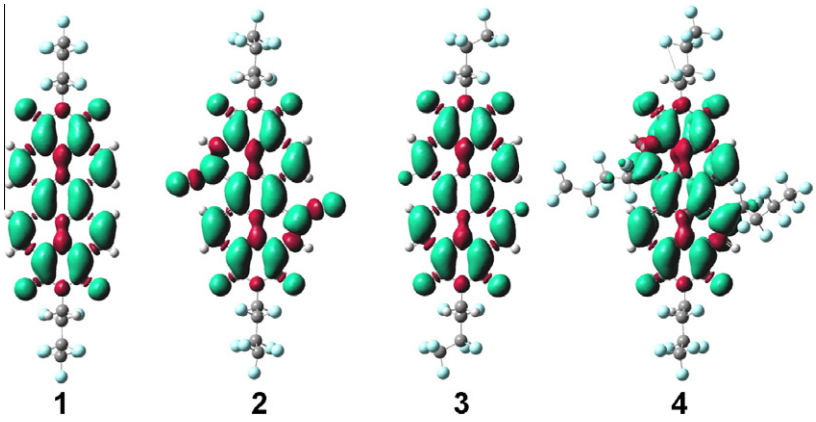

Fig. 4. Spin density distribution of the anions of compound **1**–**4**.

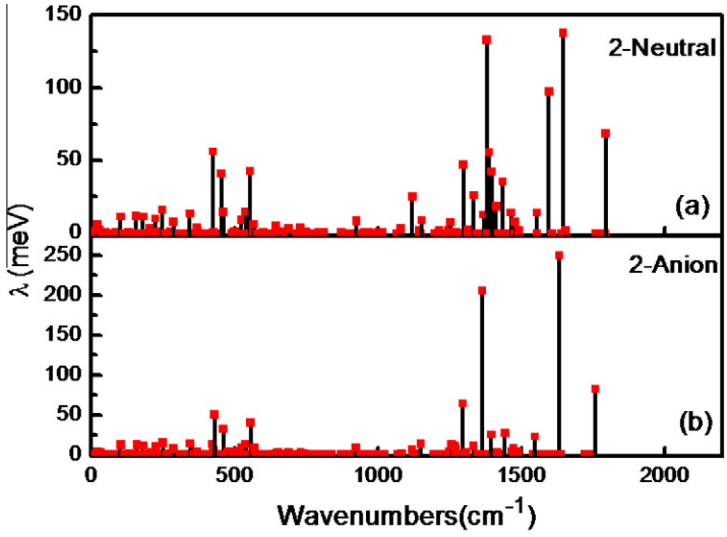

Fig. 5. Reorganization energy from NM analysis for compound **2** with the neutral state (a) and the anion state (b).

Table 2
Total reorganization energy of four compounds calculated with NM and AP methods (unit: meV).

Calculation methods	1	2	3	4
Normal mode	298	270	307	352
Adiabatic potential	298	269	306	348

of compound **1**. For comparison, the adiabatic potential energy surface (AP) method is also used to calculate the reorganization energy (see Table 2). The calculation results with the AP method agree very well with those calculated with the NM method. This fact validates the applicability of the harmonic oscillator model. From the reorganization energy analysis, compound **2** is expected to have the best charge transport properties and **4** should possess the smallest transfer rate.

The reorganization energy contributed by the core, the end substitutes and the core substitutes as well as their weights are shown in Table 3. The reorganization energy smaller than 1.0 cm^{-1} in the decomposition is ignored here. Most of the reorganization energy comes from the core for all the four systems. When the hydrogen atoms at the bay positions of the core are substituted by the CN, F and C_4F_9 groups, significant contributions to the reorganization energy from these groups are obtained. As shown in this table, the contribution from the C_4F_9 group is as high as 18.2%, much larger than the other two groups, and even larger than that from the end substitution groups. For the CN substitute, its contribution to the reorganization energy is much smaller. More importantly, it reduces the reorganization energy from both the core and the end substitutes. In our opinion, the existence of the π bond in the CN group can promote the delocalization of the electrons in the molecule, which implies that the molecular conformation will relax a little when an external charge is located on it. In addition, the nonbonding characteristic on the CN group also implies little contributions to the reorganization energy. Although the freedom of the substitute group F is the smallest, its contribution to the reorganization energy

Table 3
Decomposition of the reorganization energy of four systems on the core (except the substitute groups), the end substitution groups and the core substitution groups.

Compound		1	2	3	4
Core	R-Energy (cm^{-1})	1066.0714	998.6718	1040.257	1034.7069
	Weight	91.0%	90.5%	86.1%	69.4%
End substitutes	R-Energy (cm^{-1})	104.9363	76.9268	118.7076	184.4001
	Weight	9.0%	7.0%	9.8%	12.4%
Core substitutes	R-Energy (cm^{-1})	<1.0	28.3428	49.4987	271.1156
	Weight	–	2.5%	4.1%	18.2%

is more than we expected, which might be induced by the strong electronegativity of the F atom.

3.4. Transfer integral

Another important factor that can influence the transfer rate is the electron coupling or the transfer integral. It has been discovered that the transfer integral depends on the relative positions of the two sites involved. For different systems, the relative positions of the two sites involved are totally different owing to different stacking structures in their crystal structures. Based on the crystal structures of the four systems, the electron transfer pathways are illustrated in Figs. 6 and 7. It is worth to notice that both **1** and **2** adopt the π stacking configurations, but the displacements of the stacking pairs along the short-axis and the long-axis as well as the vertical distances are different in different transfer pathways. It is straightforward to see that the overlap between the dimers in all the pathways of **2** become larger than **1** along the long-axis. Along the short-axis direction, dimers in P1, P2, P5 and P6 pathways have comparable overlap for **2**, the vertical distances between the dimers in the upper four pathways are 3.38, 3.38, 3.08 and 3.08 Å. For compound **1**, the overlap of the dimers in P3 and P4 is less than that of dimers in P5 and P6 (see from the short axis direction), but the vertical distances are much narrower than the latter two dimers. Both the dimers in P3 and P4 for **2** and the dimers in P1 and P2 for **1** have none overlap though the vertical distances are so small. The transport network of **3** is characterized by the herringbone structure with one direction adopting the face to face packing and other two directions employing the face to edge stacking. The overlap for dimers with the π stacking pattern is very good both in the short-axis and long-axis directions. While the dimers with face to edge stacking stay far away from each other in the long-axis direction. The distances between the dimers both in the short-axis and long-axis directions of **4** are very far, only the dimmers in P1 and P2 have overlap to some extent. It is seen that the overlap for the dimers in P1 is much larger than that in P2, while the distances between the two parallel planes of the dimers in P1 and P2 are 5.70 and 3.42 Å respectively.

The electron coupling along different transfer pathways of the four systems are shown in Table 4. It shows that the electron coupling strongly depends on the transfer pathway. For **1**, only the stacking direction along P3 and P4 can provide significant electron coupling, which means that electrons transfer along the one-dimension direction. The same transport properties can also be found in **3**, where electrons can only transport along the π stacking direction (P5 and P6). Better transport properties are expected for **2** which have P1–P2 and P5–P6 two-dimension transport properties. For **4**, the long chain substitutions at both the bay position and the end position induce large displacement along short-axis and long-axis directions, which also results in that the electron transfer can only happen in the π stacking direction. Calculated results indicated that the electron coupling in P2 is much smaller than that in P1. It means that the electron transfer along

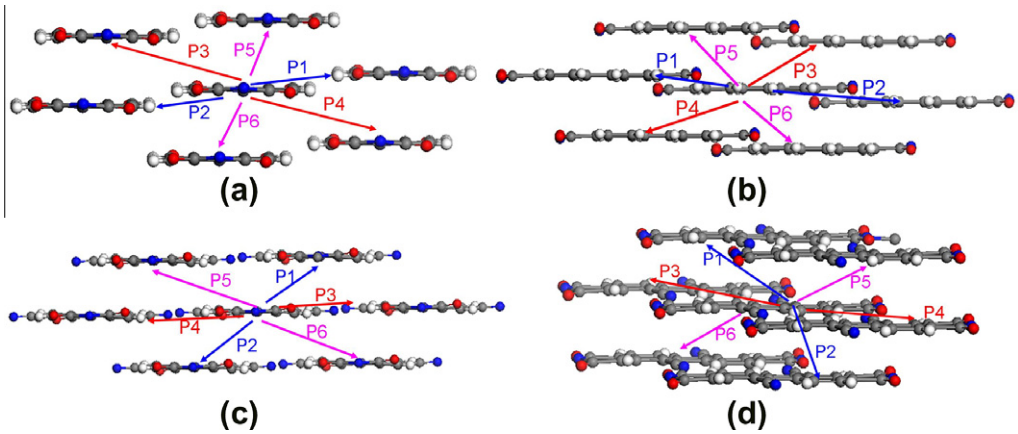

Fig. 6. Electron transfer pathways for system **1**[15] and **2**[10]; (a) short-axis view and (b) long-axis view of **1**; (c) short-axis view and (d) long-axis view of **2**. All the alkyl chain substitutions at the end of molecules are deleted for the convenience of view.

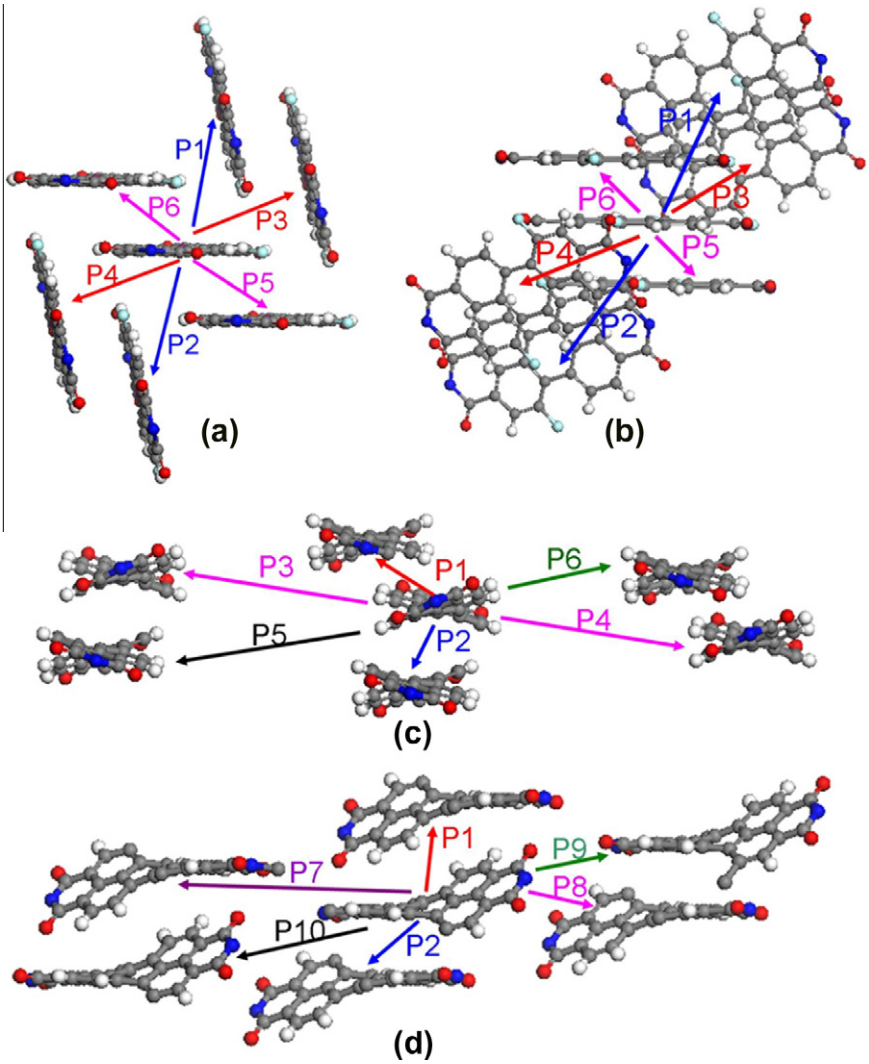

Fig. 7. Electron transfer pathways for system **3**[14] and **4**[17]: (a) short-axis view and (b) long-axis view of **3**; (c) short-axis view and (b) long-axis view of **4**. All the alkyl chain substitutions at the end of molecules are deleted for the convenience of view. The alkyl chains at the side positions of **4** are also ignored here.

Table 4
Electron coupling along different transfer pathways of four systems (unit: meV).

Pathways	1	2	3	4
P1	5.55	67.94	−1.58	−84.32
P2	5.55	67.94	−1.58	27.75
P3	−39.44	−4.57	−1.58	0.00
P4	−39.44	−4.57	−1.58	0.00
P5	−0.23	−84.74	110.29	0.00
P6	−0.23	−84.74	110.28	0.00

the π stacking direction is not very easy, although the electron coupling along P1 is as large as 84.32 meV.

3.5. Electron mobility

Based on the above calculation of the charge transfer rate along the four different paths, the kinetic Monte Carlo approach is adopted to simulate the electron transfer process in organic single crystal systems. The squared displacement versus the transport time is shown in Fig. 8. It is found that for an individual trajectory, the displacement is quite disordered. But the average value over a large number of trajectories follows a quite liner relationship with respect to time. The diffusion constant is calculated as the slope of the straight line. The average mobility is calculated based on the Einstein equation with values shown in Table 5. It is shown that the calculated values are about 2 times larger than the largest experimental results reported so far for both **1** and **2**. Owing to the extensive research on **1** and **2**, the experimental values should be reliable and our calculated results can accurately predict the relative transport properties of these systems. In this paper, many complex factors have been neglected, such as the electric field, the interface between active layer and the gate, and the charge carrier density. These factors

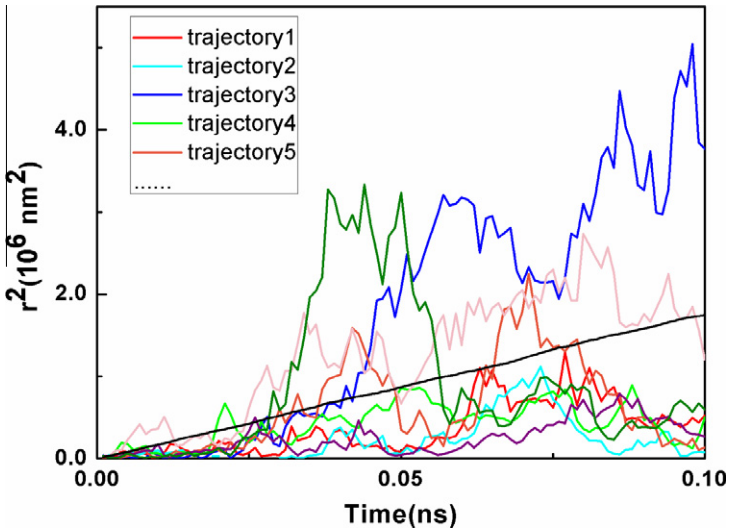

Fig. 8. Charge transport trajectories versus time. The straight line is the average values of the square displacements versus time.

Table 5
Calculated and experimental mobility of four systems (unit: $cm^2/V\,s$).

Mobility	1	2	3	4
Calculated	3.89	16.96	8.32	0.41
Experimental	1.44[15]	6[13]	0.66[15]	0.003[17]

will also play important roles in practical OFET device and their effect on the charge transport properties are quite complicated especially when they are tangled together [37,38]. Thus, it is reasonable that there is some discrepancy between the theoretical simulations and the experimental results when only the ideal crystals are considered and the intrinsic transport properties are focused here. The study on the intrinsic transport properties aims to guide the design of new functional materials. For **3** and **4**, the calculated mobility is much larger than the experimental values reported. Based on our calculations, **3** is expected to have larger mobility than **1**. It is also very possible to get larger mobility for **4** by optimizing the fabrication technique of the organic field effect transistor.

3.6. Temperature dependence

The temperature dependence of the charge mobility is an important property of organic molecular materials. It is commonly believed that the mobility decreases with temperature is a sign of the band transport mechanism.

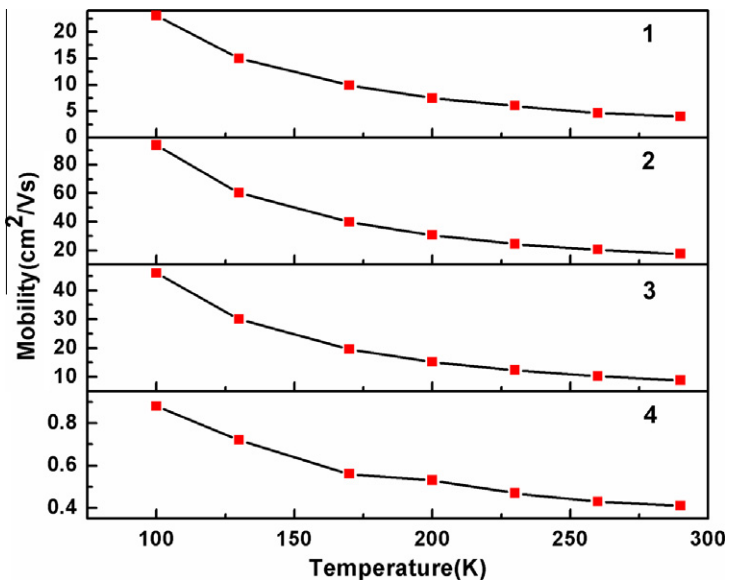

Fig. 9. Temperature dependence of the mobility of four kinds of n-type organic molecular crystals.

Indeed, for many closely packed organic single crystal materials, the charge transport does behave like band electron such as C8-BTBT [39], TMTSF [40], and rubrene [41,42]. All those organic molecular materials mentioned above are p-type materials. Very recently, the temperature dependence of the mobility of the n-type organic molecular materials (system **2**) have been investigated experimentally and the "band-like" characteristic was found from 230 K to the room temperature [43]. We also performed theoretical simulations of the temperature dependence of the mobility of system **2** and other three kinds of organic molecular crystals. The calculated mobility reduces with the increase of the temperature (see Fig. 9). All the four n-type organic molecular single-crystals under investigations present the "band-like" temperature dependence of the mobility. This is contradictory since our assumption for charge transport is based on localized charge hopping instead of band. As we have shown previously, this is purely nuclear tunneling effect appeared in Eq. (1) [21,22]. Namely, charge is still localized in a single molecule. However, since it is strongly coupled with high frequency vibration mode, it gives rise to remarkable quantum effect ($\frac{1}{2}\hbar\omega > k_B T$). This picture is in good agreement with a recent experiment observation [41] that (i) the optical spectrum for the working OFET device made of TIPS-pentacene showed localized charge feature even at temperature as low as 43 K, but (ii) the charge transport mobility at large bias decreases with temperature, much as delocalized band. Our model based on "tunneling enabled hopping" can explain such paradoxical phenomena [21]. Of course, other explanation such as the dynamics disorder based on the delocalized band picture has also shown its reasonableness [44]. However, for our investigated systems, the reorganization energy is much higher than the electronic coupling, therefore, we eliminate this possibility. It should be noted that in the experiment of Minder et al. [43], for lower temperature (T < 210 K), the mobility behaves like an thermally activated process. That is due to charge trap, commonly existed in organic materials at low temperature, which is not intrinsic property, and should not be compared with Fig. 8.

4. Conclusion

To conclude, we have investigated the electron transport properties of four kinds of substituted perylene diimides based n-type organic semiconductors by a "tunneling enabled hopping" model coupled with quantum chemistry calculations. It is found that the electron-withdrawing substitutions at the bay positions of core in the PDCDI molecules can induce the significant change of the geometric structures as well as the electronic structures of the molecule. The reorganization energy and the transfer integral have also been influenced, which induced the drastic change of the electron mobility. Our calculations strongly suggest that the cyano group (CN) is a promising substitution that not only can reduce the reorganization energy by enhancing the delocalization of the electrons, but also can make the stacking conformation favorable for electrons to transport. It is noted that the long chain perfluoroalkyl is not a preferable substitution group to increase the charge mobility. The "band-like" temperature dependence of the mobility of the four kinds of n-type organic molecular materials have been found theoretically, even though our model is based on localized charge hopping. This is ascribed to the nuclear tunneling effect. Both the temperature dependence and the mobility value at room temperature are in good agreement with the recent experiment by Minder et al. [43] for the cyano substitution.

Acknowledgement

This work is supported by National Natural Science Foundation of China (Grant Nos. 90921007, 20920102031) and the Ministry of Science and Technology through 973 program (Grant Nos. 2009CB623600, 2010CB923300, 2011CB932304, 2011CB808405), and the Goran Gustafsson Foundation for Research in Natural Sciences and Medicine, and the Swedish National Infrastructure for Computing (SNIC).

References

[1] T. Kelley, D. Muyres, P. Baude, T. Smith, T. Jones, High Performance Organic Thin Film Transistors, vol. 771, Cambridge Univ. Press, 2003.
[2] H. Klauk, U. Zschieschang, R. Weitz, H. Meng, F. Sun, G. Nunes, D. Keys, C. Fincher, Z. Xiang, Organic transistors based on di(phenylvinyl)anthracene: performance and stability, Advanced Materials 19 (22) (2007) 3882–3887.
[3] O. Jurchescu, M. Popinciuc, B. van Wees, T. Palstra, Interface-controlled, high-mobility organic transistors, Advanced Materials 19 (5) (2007) 688–692.
[4] Y. Zhang, H. Dong, Q. Tang, Y. He, W. Hu, Mobility dependence on the conducting channel dimension of organic field-effect transistors based on single-crystalline nanoribbons, Journal of Materials Chemistry 20 (33) (2010) 7029–7033.
[5] Y. Wang, R. Kumashiro, R. Nouchi, N. Komatsu, K. Tanigaki, Influence of interface modifications on carrier mobilities in rubrene single crystal ambipolar field-effect transistors, Journal of Applied Physics 105 (12) (2009) 124912–124912-5.
[6] D. Shukla, S. Nelson, D. Freeman, M. Rajeswaran, W. Ahearn, D. Meyer, J. Carey, Thin-film morphology control in naphthalene-diimide-based semiconductors: high mobility n-type semiconductor for organic thin-film transistors, Chemistry of Materials 20 (24) (2008) 7486–7491.
[7] T. Anthopoulos, B. Singh, N. Marjanovic, N. Sariciftci, A. Ramil, H. Sitter, M. Colle, D. de Leeuw, High performance n-channel organic field-effect transistors and ring oscillators based on c fullerene films, Applied Physics Letters 89 (2006) 213504.
[8] J. Na, M. Kitamura, Y. Arakawa, High performance n-channel thin-film transistors with an amorphous phase c60 film on plastic substrate, Applied Physics Letters 91 (19) (2007) 193501–193501–3.
[9] M. Kitamura, S. Aomori, J. Na, Y. Arakawa, Bottom-contact fullerene c thin-film transistors with high field-effect mobilities, Applied Physics Letters 93 (2008) 033313.
[10] B. Jones, M. Ahrens, M. Yoon, A. Facchetti, T. Marks, M. Wasielewski, High-mobility air-stable n-type semiconductors with processing versatility: dicyanoperylene-3,4: 9,10-bis (dicarboximides), Angewandte Chemie 116 (46) (2004) 6523–6526.
[11] B. Jones, A. Facchetti, M. Wasielewski, T. Marks, Tuning orbital energetics in arylene diimide semiconductors. Materials design for ambient stability of n-type charge transport, Journal of the American Chemical Society 129 (49) (2007) 15259–15278.
[12] M. Kitamura, I. Ohkubo, M. Matsunami, K. Horiba, H. Kumigashira, Y. Matsumoto, H. Koinuma, M. Oshima, Electronic structure characterization of lanimno epitaxial thin films using synchrotron-radiation photoelectron spectroscopy and optical spectroscopy, Applied Physics Letters 94 (2009) 262503.
[13] A. Molinari, H. Alves, Z. Chen, A. Facchetti, A. Morpurgo, High electron mobility in vacuum and ambient for pdif-cn2 single-crystal transistors, Journal of the American Chemical Society 131 (7) (2009) 2462–2463.

[14] R. Schmidt, M. Ling, J. Oh, M. Winkler, M. Konemann, Z. Bao, F. Wrthner, Core-fluorinated perylene bisimide dyes: air stable n-channel organic semiconductors for thin film transistors with exceptionally high on-to-off current ratios, Advanced Materials 19 (21) (2007) 3692–3695.
[15] R. Schmidt, J. Oh, Y. Sun, M. Deppisch, A. Krause, K. Radacki, H. Braunschweig, M. Konemann, P. Erk, Z. Bao, High-performance air-stable n-channel organic thin film transistors based on halogenated perylene bisimide semiconductors, Journal of the American Chemical Society 131 (17) (2009) 6215–6228.
[16] H. Usta, C. Risko, Z. Wang, H. Huang, M. Deliomeroglu, A. Zhukhovitskiy, A. Facchetti, T. Marks, Design, synthesis, and characterization of ladder-type molecules and polymers. Air-stable, solution-processable n-channel and ambipolar semiconductors for thin-film transistors via experiment and theory, Journal of the American Chemical Society 131 (15) (2009) 5586–5608.
[17] Y. Li, L. Tan, Z. Wang, H. Qian, Y. Shi, W. Hu, Air-stable n-type semiconductor: core-perfluoroalkylated perylene bisimides, Organic Letters 10 (4) (2008) 529–532.
[18] F. May, V. Marcon, M.R. Hansen, F. Grozemac, D. Andrienko, Relationship between supramolecular assembly and charge-carrier mobility in perylenediimide derivatives: the impact of side chains, Journal of Materials Chemistry 21 (2011) 9538.
[19] V. Marcon, D.W. Breiby, W. Pisula, J. Dahl, J. Kirkpatrick, S. Patwardhan, F. Grozema, D. Andrienko, Understanding structure–mobility relations for perylene tetracarboxydiimide derivatives, Journal of the American Chemical Society 131 (2009) 11426.
[20] M. Delgado, E. Kim, D. Filho, J. Bredas, Tuning the charge-transport parameters of perylene diimide single crystals via end and/or core functionalization: a density functional theory investigation, Journal of the American Chemical Society 132 (10) (2010) 3375–3387.
[21] H. Geng, Q. Peng, L.J. Wang, H.J. Li, Y. Liao, Z.Y. Ma, Z.G. Shuai, Toward quantitative prediction of charge mobility in organic semiconductors: tunneling enabled hopping model, Advanced Materials 24 (26) (2012) 3568.
[22] G. Nan, X. Yang, L. Wang, Z. Shuai, Y. Zhao, Nuclear tunneling effects of charge transport in rubrene, tetracene, and pentacene, Physical Review B 79 (11) (2009) 115203.
[23] L.J. Wang, Q.K. Li, Z.G. Shuai, L.P. Chen, Q. Shi, Multiscale study of charge mobility of organic semiconductor with dynamic disorders, Physical Chemistry Chemical Physics 12 (13) (2010) 3309.
[24] B. Paulson, L. Curtiss, B. Bal, G. Closs, J. Miller, Investigation of through-bond coupling dependence on spacer structure, Journal of the American Chemical Society 118 (2) (1996) 378–387.
[25] F. Grozema, P. Van Duijnen, A. Yuri, M. Ratner, L. Siebbeles, Intramolecular charge transport along isolated chains of conjugated polymers: effect of torsional disorder and polymerization defects, Journal of Physical Chemistry B 106 (32) (2002) 7791–7795.
[26] J. Bredas, D. Beljonne, V. Coropceanu, J. Cornil, Charge-transfer and energy-transfer processes in conjugated oligomers and polymers: a molecular picture, Chemical Reviews 104 (11) (2004) 4971–5004.
[27] K. Senthilkumar, F. Grozema, F. Bickelhaupt, L. Siebbeles, Charge transport in columnar stacked triphenylenes: effects of conformational fluctuations on charge transfer integrals and site energies, Journal of Chemical Physics 119 (2003) 9809.
[28] V. Lemaur, D. da Silva Filho, V. Coropceanu, M. Lehmann, Y. Geerts, J. Piris, M. Debije, A. van de Craats, K. Senthilkumar, D. Laurens, Charge transport properties in discotic liquid crystals: a quantum-chemical insight into structure–property relationships, Journal of the American Chemical Society 126 (10) (2004) 3271–3279.
[29] E. Valeev, V. Coropceanu, D. da Silva Filho, S. Salman, J. Brdas, Effect of electronic polarization on chargetransport parameters in molecular organic semiconductors, Journal of the American Chemical Society 128 (30) (2006) 9882–9886.
[30] A. Troisi, G. Orlandi, Hole migration in dna: a theoretical analysis of the role of structural fluctuations, Journal of Physical Chemistry B 106 (8) (2002) 2093–2101.
[31] X. Yang, L. Wang, C. Wang, W. Long, Z. Shuai, Influences of crystal structures and molecular sizes on the charge mobility of organic semiconductors: oligothiophenes, Chemistry of Materials 20 (9) (2008) 3205–3211.
[32] L. Wang, G. Nan, X. Yang, Q. Peng, Q. Li, Z. Shuai, Computational methods for design of organic materials with high charge mobility, Chemical Society Reviews 39 (2) (2009) 423–434.
[33] M. Frisch, G. Trucks, H. Schlegel, G. Scuseria, M. Robb, J. Cheeseman, G. Scalmani, V. Barone, B. Mennucci, G. Petersson, Gaussian 09, revision a. 02; gaussian, Inc., Wallingford, CT, 2009.
[34] J. Reimers, A practical method for the use of curvilinear coordinates in calculations of normal-mode-projected displacements and duschinsky rotation matrices for large molecules, Journal of Chemical Physics 115 (20) (2001) 9103–9109.
[35] H. Geng, Y. Niu, Q. Peng, Z. Shuai, V. Coropceanu, J. Brdas, Theoretical study of substitution effects on molecular reorganization energy in organic semiconductors, Journal of Chemical Physics 135 (2011) 104703.
[36] M.-Y. Kuo, H.-Y. Chen, I. Chao, Cyanation: providing a three-in-one advantage for the design of n-type organic field-effect transistors, Chemistry C: A European Journal 13 (17) (2007) 4750–4758.
[37] S. Yin, Y. Lv, Modeling hole and electron mobilities in pentacene ab-plane, Organic Electronics 9 (2008) 852–858.
[38] S. Yin, Y. Yang, Y. Lv, Theoretical study the trap and carrier-density dependent electron mobility in pentacene ab-plane by the steady master equation, Synthetic Metals 160 (2010) 1241–1246.
[39] C. Liu, T. Minari, X. Lu, A. Kumatani, K. Takimiya, K. Tsukagoshi, Solution-processable organic single crystals with bandlike transport in field-effect transistors, Advanced Materials 23 (4) (2011) 523–526.
[40] H. Xie, H. Alves, A.F. Morpurgo, Quantitative analysis of density-dependent transport in tetramethyltetraselenafulvalene single-crystal transistors: intrinsic properties and trapping, Physical Review B 80 (24) (2009) 245305.
[41] I.N. Hulea, S. Fratini, H. Xie, C.L. Mulder, N.N. Iossad, G. Rastelli, S. Ciuchi, A.F. Morpurgo, Tunable frohlich polarons in organic single-crystal transistors, Nature Materials 5 (12) (2006) 982–986, http://dx.doi.org/10.1038/nmat1774.
[42] V. Podzorov, E. Menard, A. Borissov, V. Kiryukhin, J.A. Rogers, M.E. Gershenson, Intrinsic charge transport on the surface of organic semiconductors, Physical Review Letters 93 (8) (2004) 086602. pRL.
[43] N. Minder, S. Ono, Z. Chen, A. Facchetti, A. Morpurgo, Band-like electron transport in organic transistors and implication of the molecular structure for performance optimization, Advanced Materials 24 (4) (2012) 503–508.
[44] A. Troisi, Dynamic disorder in molecular semiconductors: charge transport in two dimensions, Journal of Chemical Physics 134 (2011) 034702.